**Responses to reviewers' comments on**
**"Tomographic reconstruction of atmospheric gravity wave parameters from airglow observations" by Song et al.**

The authors would like to thank the reviewers for their valuable comments, which helped us to improve the quality of this manuscript. We have addressed all the comments, and the reply to each comment is highlighted in blue as follows.

**Reply to Anonymous Referee #1**

The paper "Tomographic reconstruction..." by R. Song et al. describes a new variant of a tomographic retrieval which is custom tailored to a not-yet existing measurement system planned to be operated in a novel measurement mode. As a methodical preflight-study the scope of the paper fits well in AMT but a couple of details should be clarified prior to publication. In general, the paper is well written, well organized, scientifically sound, and as far as I can judge, all relevant literature has been referenced.

We thank the referee for carefully reviewing the manuscript and for the positive comments.

Scientific issues:

p2 l30: I am not quite sure if the term "oversampling" is adequate here, at least in the context of MIPAS (although MIPAS is not explicitly mentioned here, the Carlotti et al. reference hints at MIPAS). Von Clarmann et al., Atmos. Meas. Techn., Vol. 2(1), 47-54, 2009, "The horizontal resolution of MIPAS", find that the horizontal resolution of MIPAS in terms of along-track information smearing is better than the horizontal sampling in terms of the horizontal spacing of measurement geo-locations. Thus there is undersampling, not oversampling. Either reword, or define clearly in which sense you use the admittedly ambiguous term "oversampling". Does it refer to the retrieval space or the measurement space, etc?

Thanks for the suggestion. We agreed that the term "oversampling" is inadequate here. The original meaning of this sentence is to show that better horizontal resolution can be achieved for some limb sounders, such as MLS and MIPAS. As such instruments observe the atmosphere along the track of the orbit, the atmospheric variability along the LOS can be considered in the retrieval. In the paper "The horizontal resolution of MIPAS" by Von Clarmann et al., the authors explained clearly that the along-track smearing is two times smaller than the horizontal sampling, which means the atmosphere is undersampled. Therefore, we have rewritten this sentence and added the reference of Von Clarmann et al. "...mitigate this general limitation by considering the horizontal variability of the atmosphere in the retrieval (Livesey and Read, 2000; Carlotti et al., 2001; von Clarmann et al.,2009)".

p5 l5 and p8 l15: On page 5 the atmosphere is assumed to be so opaque that any signal from the lower atmosphere and surface can be ignored. On page 8 the atmosphere is so optically thin that no self-absorption has to be considered. These two approximations seem to be in conflict with each other, except if the transmission jumps from 1 to 0 at the target air volume. I do not doubt that the approximations made can somehow be justified but I think that a little more discussion is needed to refute the apparent contradiction. Particularly in the sub-limb mode I expect that you either get considerable signal from altitudes below the target volume, or that the atmosphere in front/above the target volume is not really transparent.

In the infrared, this model assumes the atmosphere to be optically thick in the lower atmosphere and optically thin in the upper atmosphere. To avoid the conflict in the manuscript, we added a sentence to explain the assumption prior to use: "In the infrared the lower atmosphere is optically thick, whereas the upper atmosphere can be considered as optically thin. Since the $O_2$ A-Band is a transition to the $O_2$ ground state, the atmosphere becomes optically thick at stratopause altitudes. Therefore, any emission from the Earth's surface or tropospheric altitudes cannot reach the upper mesosphere at these wavelengths. At nightglow layer altitudes (upper mesosphere / lower thermosphere) the atmosphere is optically thin for the wavelengths considered. In our case,...".

p6, general comment: No statement is made how well the measurement geometry is known, and in consequence, how well the pressures at the tangent points are known. The measured signal does not only depend on temperature but also on the number of molecules along the ray-path (or more precisely: the transparent and semi-transparent part of the ray-path). How is this multi-variable problem solved? Or is the tacit assumption made that the actual measurement geometry and pressure distribution are perfectly known? The manuscript should be a bit clearer with respect to this.

Thanks for the suggestion. In this simulation, the pressure is not needed and the actual measurement geometry is assumed perfectly known. The atmospheric temperature $T$ is retrieved on the tangent altitudes in this study.

Wording and presentation issues and technical corrections:

Abstract: About a third of the abstract are like an introduction. I would prefer an abstract which includes less general introductory information but more methodical information and or results.

Thanks. We have revised the abstract according to your suggestion.

p1 l10: There is no "2-dimensional atmospheric state". Better say "allow for tomographic 2-dimensional reconstruction of the atmospheric state".

Agreed. This change has been made.

p1 l11: "As no real data are available" sounds too defensive to my ears. It is fully legitimate to present pre-flight studies and retrieval sensitivity studies in AMT. Why not simply "The feasibility of this tomographic retrieval approach is assessed using simulated measurements".

Thanks for the suggestion. This sentence has been rewritten.

p1 l12: "much smaller" than what?

The text has been revised to clarify this. "It shows that one major advantage of this observation strategy is that GWs can be observed on a much smaller scale than conventional observations."

p1 l20: comma after "(GWs)"

A comma has been added after "(GWs)".

p2 l14 "they include": not quite clear what "they" refers to. I suggest to reword.

This sentence has been reworded. "GWs can be also characterized by nadir viewing instruments, such as the Atmospheric Infrared Sounder (AIRS) (Alexander and Barnet, 2007; Hoffmann and Alexander, 2009; Ern et al., 2017) and the Advanced Microwave Sounding Unit (AMSU) (Wu, 2004)".

p3 l2 "limited-angle tomography". This sounds as if it was a technical term but I have never heard it before. Please either define this technical term, or avoid it and use generic terms instead.

This sentence has been rewritten to clarify this point. "This results in multi-angle observations of the target volume, such that a tailored retrieval scheme can be applied. This differs from classical limited-angle tomography, where only observations within a limited angular range are taken for the reconstruction."

p3 l3/4: The technical term "target mode" is used here twice but defined only in line 18. I suggest to write "In Section 2 we present the observation strategy which we call ‘target mode’ observations. Then it is clear that you give this name to something new and the reader will not wonder if he/she has missed anything.

Thanks for the suggestion. This sentence has been revised.

p3 l 16: Please define the term "sub-limb sounding".

The term "sub-limb" has been defined in text. "The sub-limb sounding has a similar geometry with limb sounding, whereas the tangent heights are near or below the surface."

p3 l 23: The description of the geometry is somewhat unclear. You talk about "limb sounding", not "limb imaging". This implies that during one limb scan the viewing geometry is changing all the time. It is thus not clear how multiple consecutive profiles can be obtained while a limb view is kept. The text would be much clearer if you distinguish between limb scanning (usually used as a synonym to limb sounding) or limb imaging (recording of multiple ray-paths at the same time) is used. The statement "The instrument will keep the limb view" currently has three possible different meanings: 1. A series of measurements is made using the SAME tangent altitude. 2. A profile of limb radiances is measured simultaneously with a 1D imaging device. 3. Tangent altitudes change while the limb is scanned, and the statement is just meant to tell me that it is not switched from the limb-scanning mode to the sub-limb mode. Please clarify. Perhaps use a weaker wording than "will keep this limb view"; perhaps say "The instrument will continue to measure under limb geometry for a period of time"; and finally clarify what type of "vertical profiles" are measured. I guess "vertical radiance profiles".

Thanks for finding and explaining this point that was not clear in the manuscript. We have revised this paragraph to avoid misleading the readers. First, the term "limb sounding" has been replaced by "limb imaging". Second, we accepted your suggestion for revising the sentence "The instrument will keep this limb view...". It has been rewritten as "The instrument will continue to measure under limb geometry for a period of time, and multiple consecutive vertical radiance profiles will be taken during this time".

p5 l18: Is A1 really a "transmission probability" or do you mean a "transition probability".

Corrected as "transition probability".

p6 l2: Is the A1 here the same as in Eq 3: Please use different symbols for different designates, and/or use the same technical terms for the same designates.

In Eq 3, the A-band transition probability is represented by $A_1$. In Eq 6, the wave amplitude is represented by $A$.

p8 Eq 13: Since $\mathbf{S}_a^{-1}$ is not the inverse of a covariance matrix but a freely defined regularization term, I find it inadequate to use the symbol Sa here, which is usually applied only for probabilistic a priori covariance matrices.

Thanks for the suggestion. Therefore, we use $\mathbf{R}$ instead of $\mathbf{S}_a^{-1}$ in Eq 13 and the following text.

p9 l2: Not clear what "It" refers to. The content suggests that it refers to the entire regularization procedure but grammatically it refers to the a priori data alone, which does NOT ensure that a unique solution can be obtained. I suggest: "The second term in the cost function (Eq. 13) ensures that..."

Agreed. This sentence has been revised to : "The second term in the cost function (Eq. (13)) ensures that..."

p9 l5: references to Levenberg, Marquardt, and the implementation actually used would be appropriate.

Relevant references have been added. "(Levenberg, 1944; Marquardt, 1963; Ceccherini and Ridolfi, 2010)".

p9 l11: you may wish to add the term "unstable solution" here

Accepted. Sentence has been revised as "... while a small value will give an unstable solution".

p10 Eq 16: If you used the convention that $\boldsymbol{f}' = \mathbf{K}$, then the equation would be easier to recognize (and, of course, define K prior to its use).

Agreed. $\boldsymbol{f}'$ has been replaced by $\mathbf{K}$ for easier recognition. A sentence has been added to define $\mathbf{K}$: "where $\mathbf{K}$ is the Jacobian of the forward model $\boldsymbol{f}$ at atmospheric state $\boldsymbol{x}$".

p10 l20: For the non-specialist it would be helpful to clarify if you perturb the temperature field only or if you adjust pressure (and with this also absolute concentrations of species) hydrostatically.

A sentence has been added to clarify this: "The temperature, atmospheric density and concentrations of various constituents are perturbed by this simulated wave."

p14 l17: Has the acronym LOS already been defined? With respect to the "poor horizontal resolution", see my comment on p2 l30: At least for MIPAS it is the horizontal sampling and not the resolution of the measurement itself which is limiting the horizontal resolution of the data product.

The acronym LOS is defined in p3 l30 (discussion paper): "Figure. 2 shows how the line-of-sights (LOSs) of...". With respect of the "poor horizontal resolution", this point has been revised in the introduction according to the comment on p2 l30.

**Reply to Anonymous Referee #2**

This manuscript thoroughly describes a methodology of retrieving 3D gravity wave parameters (wavelength and amplitude) from a synthetic remote sensing instrument that is designed to work on the “target mode” at O2 A-band. Taking the advantage of combining both “limb” and “sub-limb” strengths, this “target mode” can capture the majority of the gravity waves on the spectrum except the very small ones (both horizontal and vertical wavelengths are small). The aiming region is at mesopause where a lot of gravity wave breaking and secondary generation occur, so this methodology, together with the specially designed viewing geometry, is likely a powerful tool of investigating the gravity wave dynamics, and mesosphere-thermosphere coupling on a global scale. This paper is well-written. The flow is smooth, the logic is strict, and the presentation is concise and clear. It well suits the journal of AMT, and deserves a final publication. I have some broad questions and comments that I hope the authors can address before final publication. I don’t want to hit the "major revision" button because the following comments are indeed not too critical. But I sincerely hope the authors could take at least #3 seriously and add one figure to address this issue.

We thank the reviewer for providing a thorough review and offering valuable suggestions. We have revised the manuscript according to the comments. Especially for #3, an additional figure has been used to clarify the problem.

1. Although the “observation” is synthetic, the paper is not clear about what the designed orbit, scan frequency, global coverage, etc. should be, so readers have no idea whether this “mission”, if successfully launched, could be suitable for case studies

and climate studies

Thanks for the suggestion. A few sentences have been added in the beginning of Sect 5.2 to clarify this:
" The satellite platform is simulated in an approximately 600 km sun-synchronous orbit with an inclination angle of 98°. The instrument will employ a 2D detector array consisting of about 40 × 400 super pixels. It measures in the spectral regions from 13082 to 13103 $cm^1$ within the altitude range from ≈60 to 120 km in limb imaging measurements.".

2. Similar to the above question, the integration time of each limb/sub-limb view seems to impact the sensitivity window (i.e., Fig. 8). Other than gain (or signal-noise ratio), I don't see a clear way that they are connected. Can you quantitatively elaborate why?

Yes, the integration time will affect the sensitivity window as shown in Fig. 8. The sensitivity to horizontal waves can be increased by using shorter integration time. The shorter the integration time is, the less horizontal information of the atmosphere will be smoothed in each limb or sub-limb view. However, this integration time should also be adequate such that enough photons can be received by the instrument. In this experiment we aim to show the readers that, for the same instrument the horizontal resolution can be improved by incorporating sub-limb measurements, even if the integration time of the instrument itself can not be improved. For this reason, we didn't show the influence of integration time on the sensitivity window in Fig. 8. Then it's clear to see how the 'target mode' can improve the performance in analyzing horizontal wavelength of the waves.

3. The authors mentioned that one of the difficulty this "target mode" can conquer is that we don't need two adjacent orbits to determine the horizontal wavelength. But in my understanding, the aliasing effect still exists, i.e., the satellite instrument is still only sensitive to wave fronts that are parallel to the LOS. In the "pseudo-retrieval", the input "truth" is also a linear gravity wave with wave front parallel to the LOS. What about other direction? I think an evaluation of the dependence of retrieved wave parameter as a function of wave vector direction is necessary to show to the readers. In addition, it would be nice to briefly discuss the situation of a mixture of two linear waves, and other types of GWs, e.g., circular rings. The general interests lie in the fact that many GWs become non-linear at the mesopause.

Agreed. In this 'target mode', the instrument is sensitive to the wave vector that has a component parallel to the LOS. This effect was not clarified in the manuscript. We added a figure to illustrate the viewing geometry between the LOS and wave vector. A few sentences were used to clarify this effect before the results of the sensitivity study are presented:
"For this 'target mode', the observed horizontal wavelength is the wavelength projected along the LOS. In general, there is an angle $\alpha$ between the LOS and the horizontal wave vector. Therefore, the observed horizontal wavelength $\lambda_x$ is a factor of $1/(\cos\alpha)$ larger than the real horizontal wavelength $\lambda_r$, as illustrated in the added figure. In this sensitivity study, the horizontal wavelength discussed is the observed horizontal wavelength $\lambda_x$".
The focus of this paper is to show how well the horizontal resolution can be improved by performing the 'target mode' observation. In the case of 2-dimensional retrieval, a combination of vertical and horizontal information is enough for the analysis of any 2-d waves. We are currently working on another retrieval strategy to get more information on the orientation of the wave vector. However, this topic is rather complex and would fill another paper.

4. Regarding the horizontal wavelength, there is still no way to decompose it to lambda_x and lambda_y, is that right?

Yes, right. This point has been clarified in Comment #3.

Minor points: P1, L3: wind system -> wind structure. P1, L15: for -> from P2, L8: they include -> these datasets include P2, L10: In Wu and Waters (1996), they used the saturated radiance (and hence, it's sub-limb technique, not limb, read Wu and Eckermann (2008, JAS) for details), not the retrieved temperature. P2, L15: Please include Gong et al. [2012, ACP] and Hoffmann et al. [2016, ACP] in the reference list. P2, L23: short horizontal waves –> waves with short horizontal wavelengths. P2, L32: add "small" before "structure". P3, L19: observation -> observations.

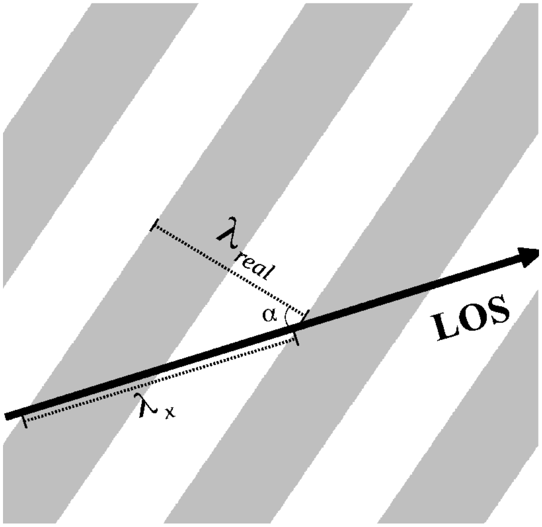


**Figure 1.** Viewing geometry between the satellite line-of-sight (LOS) and the horizontal wave vector. The wave fronts are represented by the gray shading. The observed horizontal wavelength $\lambda_x$ and the real horizontal wavelength $\lambda_{\text{real}}$ are related by an angle $\alpha$: $\lambda_{\text{real}} = \lambda_x \cos\alpha$.

Thanks for the detailed reading. All these minor points have been addressed in the revised manuscript.

Fig. 5: My understanding is that this figure shows the weighting function of each channel, correct? If that's the case, I think it's better to draw the weighting function line as a function of altitude for each channel, using different color to represent different channels would be a better idea. Right now it's not straightforward of the subtle difference of weighting function peak at different altitude.

This figure is not the weighting function for each channel. It shows the simulated radiance at different tangent heights.

# Tomographic reconstruction of atmospheric gravity wave parameters from airglow observations

Rui Song [1,2], Martin Kaufmann [1], Jörn Ungermann [1], Manfred Ern [1], Guang Liu [3], and Martin Riese [1]

[1]Institute of Energy and Climate Research, Stratosphere (IEK-7), Research Centre Jülich, 52425 Jülich, Germany
[2]Physics Department, University of Wuppertal, 42097 Wuppertal, Germany
[3]Key Laboratory of Digital Earth Sciences, Institute of Remote Sensing and Digital Earth, Chinese Academy of Sciences, Beijing, China

*Correspondence to:* R. Song (r.song@fz-juelich.de)

**Abstract.**

Gravity waves (GWs) play an important role in ~~atmospheric dynamics . Especially in~~ the dynamics of the mesosphere and lower thermosphere (MLT)~~dissipating GWs provide a major contribution to the driving of the global wind system~~. Therefore global observations of GWs in the MLT region are of particular interest. The small scales of GWs, however, pose a major problem for the observation of GWs from space. We propose a new observation strategy for GWs in the mesopause region by combining limb and sub-limb satellite-borne remote sensing measurements for improving the spatial resolution of temperatures that are retrieved from atmospheric soundings. In our study, we simulate satellite observations of the rotational structure of the $O_2$ A-band nightglow. A key element of the new method is the ability of the instrument or the satellite to operate in so called 'target mode', i.e. to stare at a particular point in the atmosphere and collect radiances at different viewing angles. These multi-angle measurements of a selected region allow for tomographic ~~reconstruction of a 2-dimensional~~ 2-dimensional reconstruction of the atmospheric state, in particular of gravity wave structures. ~~As no real data is available, the~~ The feasibility of this tomographic retrieval ~~is carried out with simulation data in this work~~approach is assessed using simulated measurements. It shows that one major advantage of this observation strategy is that ~~much smaller scale~~ GWs can be observed on a much smaller scale than conventional observations. We derive a GW sensitivity function, and it is shown that 'target mode' observations are able to capture GWs with horizontal wavelengths as short as ∼50 km for a large range of vertical wavelengths. This is far better than the horizontal wavelength limit of 100-200 km obtained ~~for~~ from conventional limb sounding.

## 1 Introduction

Miniaturization in remote sensing instrumentation as well as spacecraft technology allows for the implementation of highly focused satellite missions, for example to observe airglow layers in the mesosphere and lower thermosphere (MLT) region. The MLT extends between about 50 and 110 km in the Earth's atmosphere, and is highly affected by atmospheric waves, including planetary waves, tides and gravity waves (GWs), which are mainly excited in the lower atmosphere (Vincent, 2015). Atmospheric GWs are the main driver for the large-scale circulation in the MLT region with considerable effects on the atmospheric state and temperature structure (Garcia and Solomon, 1985; Holton, 1982; Lindzen, 1981).

Temperature is a key quantity to describe the atmospheric state, and it is a valuable indicator to identify and quantify atmospheric waves, such as GWs (e.g., Fritts and Alexander 2003, and reference therein). As GWs displace airparcels adiabatically both in vertical and horizontal directions, this process affects the temperature of the atmosphere. Assuming linear wave theory, GW-related fluctuations in different parameters (wind, temperature, density, etc.) are directly connected via the linear polarization relations (e.g., Fritts and Alexander 2003). Therefore, amplitudes, wavelengths, and phases of a GW can be determined from its temperature structure (Fritts et al., 2014; Ern et al., 2004, 2017).

Over the last few decades, data from satellite and aircraft instruments have been extensively used to characterize vertically resolved gravity wave parameters. Utilizing limb soundings, ~~they~~ these datasets include temperature or density data acquired by the Limb Infrared Monitor of the Stratosphere (LIMS) (Fetzer and Gille, 1994, 1996), the Global Positioning System (GPS) radio occultation (RO) (Tsuda et al., 2000), ~~the Microwave Limb Sounder (MLS) (Wu and Waters, 1996),~~ Cryogenic Infrared Spectrometers and Telescopes for the Atmosphere (CRISTA) (Eckermann and Preusse, 1999), Sounding of the Atmosphere using Broadband Emission Radiometry (SABER) (Ern et al., 2011; Preusse et al., 2009a), High Resolution Dynamics Limb Sounder (HIRDLS) (Alexander et al., 2008) and Gimballed Limb Observer for Radiance Imaging of the Atmosphere (GLORIA) aircraft (Riese et al., 2014; Kaufmann et al., 2015; Ungermann et al., 2010b, 2011). ~~Utilizing nadir sounding observations, they include data by~~ GWs can be also characterized by nadir viewing instruments, such as the Atmospheric Infrared Sounder (AIRS) ~~(Alexander and Barnet, 2007; Hoffmann and Alexander, 2009; Ern et al., 2017)~~ (Alexander and Barnet, 2007; Hoffmann and Alex the Advanced Microwave Sounding Unit (AMSU) (Wu, 2004).

Typical limb sounders provide middle atmosphere temperature data with a vertical resolution of 1-3 km assuming a horizontally homogeneous atmosphere. In most cases, vertical structures of small horizontal-scale GWs are characterized by separating a background temperature profile from the measured profiles. To this background temperature, the average temperature structure of the atmosphere contributes, as well as several different modes of planetary waves (e.g., Ern et al. 2009), and tides (e.g., Forbes et al. 2006). The final results of this procedure are altitude profiles of temperature perturbations due to GWs. Temperature data obtained from limb sounding instruments exhibit a very good vertical resolution, but suffer from a poor horizontal resolution along the instrument's line-of-sight, thus limiting the visibility of ~~short horizontal waves~~waves with short horizontal wavelengths. Ern et al. (2004) proposed to combine the phases provided by the wave analysis of adjacent temperature vertical profiles to estimate the horizontal wavelength of GWs. This approach has been successfully applied to retrieve GWs with vertical wavelengths between 6 and 30 km and horizontal wavelengths larger than 100 km from CRISTA-2 measurements. This method has been used also for several other datasets (Alexander et al., 2008; Wright et al., 2010; Ern et al., 2011).

A general limitation of all methods based on limb sounding is the poor along line-of-sight resolution of this kind of measurement, which is typically a few hundred kilometers. A few existing and upcoming limb sounders try to mitigate this general limitation by ~~oversampling the data in horizontal direction (Carlotti et al., 2001; Livesey and Read, 2000)~~ considering the horizontal variability of the atmosphere in the retrieval (Livesey and Read, 2000; Carlotti et al., 2001; von Clarmann et al., 2009) . The GLORIA limb sounder utilizes a tomographic reconstruction technique, which leads to a horizontal resolution of 20 km (Ungermann et al., 2010b). In this work, we present another measurement strategy to detect atmospheric small structures, whose spatial dimensions are neither covered by conventional limb sounding nor satellite- or ground based nadir sounding. It is applicable to a low-cost nanosatellite utilizing a remote sensing instrument to measure atmospheric temperature and a high precision pointing system. Simply speaking, the satellite is commanded in such a way that the instrument observes a certain volume in the atmosphere multiple times while the satellite is flying by. This results in multi-angle observations of the target volume, such that a ~~retrieval scheme which~~ tailored retrieval scheme can be applied. This differs from classical limited-angle tomography~~can be applied~~, where only observations within a limited angular range are taken for the reconstruction.

In Sect. 2, we present the observation strategy ~~of~~ which we call 'target mode' observations. Sect. 3 describes the forward modeling of such 'target mode' measurements, which is based on a 2D ray tracing, an oxygen atmospheric band (A-band) airglow emission model, a gravity wave perturbation, and the corresponding radiative transfer. The retrieval algorithm is presented in Sect. 4. In Sect. 5, the performance of the 'target mode' tomographic retrieval is tested with simulated measurements. A sensitivity study is used to analyze its performance in deriving GW fine structures compared with pure limb tomographic retrieval. The conclusion is given in Sect. 6.

## 2 Observation strategy

The detection of small scale structures in Earth's atmosphere in 2D requires new instruments or measurement strategies, as stated above. One of those is to observe atmospheric volumes from different viewing directions, e.g. by staring at one particular region while the instrument is flying by. Such tomographic retrievals have been demonstrated and implemented in a variety of measurements for different purposes, including Carlotti et al. (2001) for Michelson Interferometer for Passive Atmospheric Sounding (MIPAS), Livesey and Read (2000) for MLS, Ungermann et al. (2010a) for Process Exploration through Measurements of Infrared and millimetre-wave Emitted Radiation (PREMIER), and Ungermann et al. (2011); Kaufmann et al. (2015) for the airborne GLORIA instrument. In this work, we propose to combine satellite-borne limb and sub-limb measurements of a nightglow layer in such a way that we obtain multi-angle observations of a particular air volume as well. The sub-limb sounding has a similar geometry with limb sounding, whereas the tangent heights are near or below the surface. We name this combined observation strategy 'target mode', i.e. we adopt the same expression as for similar measurements in Earth ~~observation~~observations. In the following, the capabilities of 'target mode' observations will be discussed for a specific sequence of satellite pointing maneuvers.

Figure. 1 illustrates the viewing geometry of the 'target mode' observation, which incorporates limb and sub-limb sounding measurements. When the satellite is operated in 'target mode', the instrument will start to observe the target atmospheric volume by forward limb ~~sounding~~ imaging first. The instrument will ~~keep this limb view~~ continue to measure under limb geometry for a period of time, and multiple consecutive vertical radiance profiles will be taken during this time. Then, the instrument will switch to a forward sub-limb view with a 24.5° viewing angle below horizon. This viewing angle is also constant during the sub-limb observations. In this way, the volume will be scanned twice by the limb and sub-limb observations. Depending on the flexibility and possible speed of satellite operations more viewing angle positions could be used, for example another position with a viewing angle >24.5° as indicated in Fig. 1. After the satellite overpasses the target volume, the same measurement sequence will be applied by back-looking at the target volume.

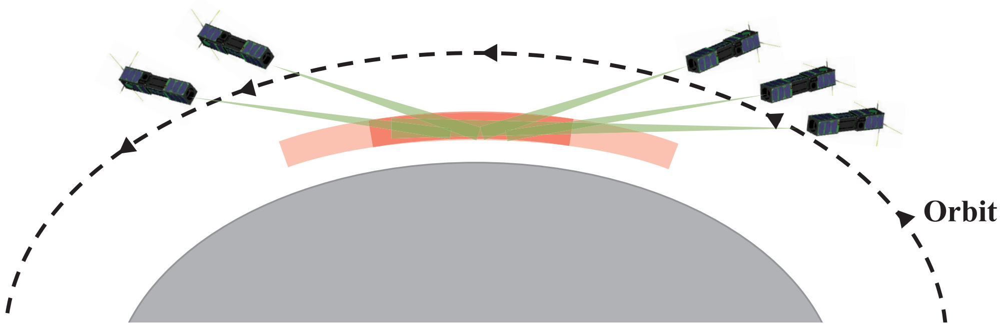


**Figure 1.** Viewing geometry of 'target mode' observations of a region in a mesospheric emission layer. This observation mode consists of forward limb, forward sub-limb and backward sub-limb measurements. The sub-limb measurements are taken with two different viewing angles, 24.5° when the satellite is far from the target region and 33° when it is relatively closer. The viewing angle is the angle relative to the instantaneous horizon, with horizon defined as Earth surface for a given but temporally changing satellite position.

Figure. 2 shows how the line-of-sights (LOSs) of the measurements overlap with each other in the orbit plane under limb sounding and 'target mode', respectively. For an assumed orbit altitude of 600 km, the corresponding measurement time for taking the measurement sequences for the limb sounding mode shown in Fig. 2 (a) is 1.6 minutes. We further assume a high measurement frequency of 10 sec per vertical profile. As can be seen from Fig. 2 (a), for the limb sounding mode the LOSs of consecutive limb profiles overlap, which means that the same atmospheric volume is observed under different directions. While in the 'target mode' (Fig. 2 (b)), sub-limb measurements contribute further information by intersecting the observed volume at different viewing angles about 3.3 minutes after the limb observations were taken.

## 3 Forward model

### 3.1 $O_2$ A-band nightglow emission model

The observation strategy presented in the previous section requires that the observed emission is restricted to a limited altitude range and that any emissions from lower parts of the atmosphere or Earth's surface cannot reach the instrument. This requires that the atmosphere below the emission layer needs to be optically thick for those emissions. This limits the number of potential airglow emissions significantly, because most of them are hotband transitions between two excited vibrational states. The number density of the lower state of a hotband transition is typically too low to absorb background radiation from the lower atmosphere. Therefore we have to search for airglow emissions, whose lower state is a ground state of a frequent atmospheric species. This is the case for the $O_2$ A-band nightglow emission. The emitting electronic state is excited in a two-step Barth process (Burrage et al., 1994; Greer et al., 1981):

$$\mathrm{O} + \mathrm{O} + \mathrm{M} \rightarrow \mathrm{O}_2^* + \mathrm{M} \tag{1}$$

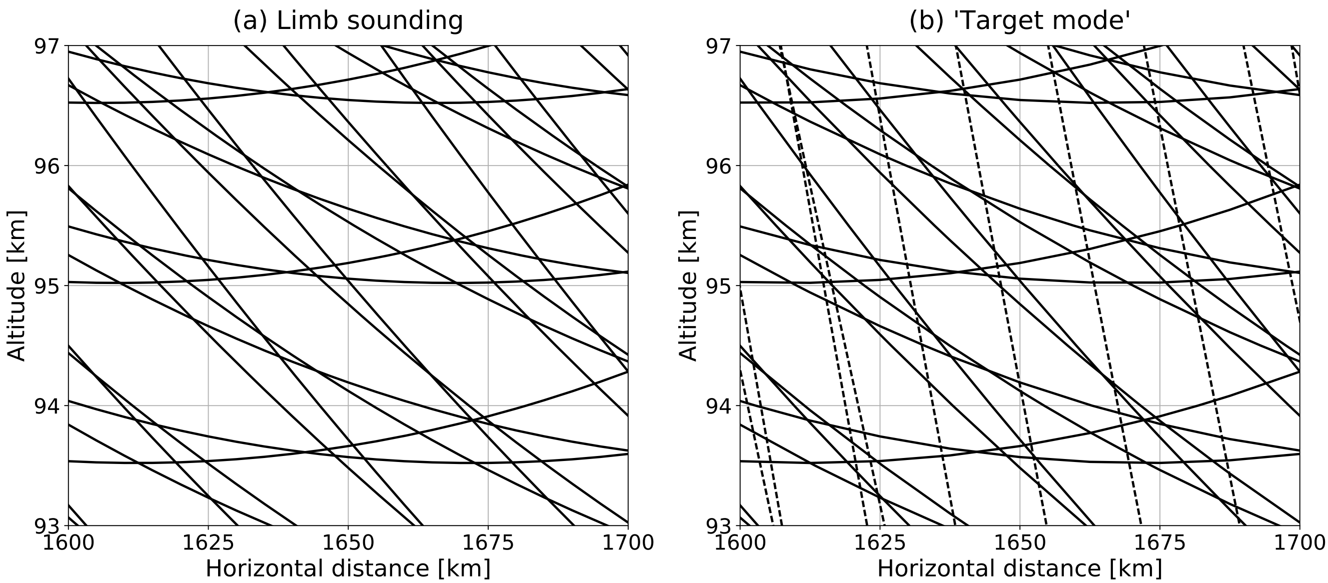


**Figure 2.** Central measurement track of an imaging instrument in the pure limb sounding and 'target mode'. The solid lines represent limb measurements and dashed lines represent sub-limb measurements. Satellite viewing geometry of Fig. 2 (b) is the same as Fig. 1.

where M is an $O_2$ or $N_2$ molecule, and $O_2^*$ is an excited $O_2$ molecule. Then, $O_2^*$ state is quenched to a lower electronic state $O_2(b^1\Sigma)$, which emits $O_2$ A-band radiation:

$$O_2^* + O_2 \rightarrow O_2(b^1\Sigma) + O_2 \tag{2}$$

Loss mechanisms for both $O_2(b^1\Sigma)$ and its undefined precursor $O_2^*$ include quenching by $O_2$, $O_3$, $N_2$ or O and spontaneous emission. The A-band volume emission rate (VER) $\eta$, in photons $\cdot\, s^{-1} \cdot cm^{-3}$, is thus (McDade et al., 1986):

$$\eta = \frac{A_1 k_1 [O]^2 [M][O_2]}{(A_2 + k_2[O_2] + k_3[N_2] + k_4[O])(C_{O_2}[O_2] + C_O[O])} \tag{3}$$

where [] refers to the number density of the species within the brackets. $A_1$ is the A-band ~~transmission~~ transition probability, $A_2$ is the total transition probability of the zeroth vibrational level of the $O_2(b^1\Sigma)$ state (Vallance Jones, 1974). $k_1$ is the reaction coefficient rate for reaction Eq. (1) (Campbell and Gray, 1973). The quenching rates for $O_2$, $N_2$ and O are denoted by $k_2$, $k_3$, and $k_4$, respectively. $C_{O_2}$ and $C_O$ describe quenching rates of $O_2^*$ by $O_2$ and O. All rate constants utilized in this work are taken from Sheese (2011). A typical vertical profile of a modeled $O_2$ A-band nightglow emission from 80-110 km is shown in Fig. 3. The temperature $T$ and number densities of $O_2$, $N_2$ and O are taken from the Hamburg Model of the Neutral and Ionized Atmosphere (HAMMONIA) (Schmidt et al., 2006) model run at 30° N and 88° E for 22:00 local solar time. The intensity of the $O_2$ A-band nightglow limb emission peaks at around 93 km; typical peak values are $3 \times 10^3$ photons $\cdot\, s^{-1} \cdot cm^{-3}$.

Since the lifetime of the $O_2(b^1\Sigma)$ state is more than 12 sec, it can be assumed that the molecule is in rotational local-thermodynamic equilibrium (Vallance Jones, 1974). This allows to derive the kinetic temperature of the atmosphere from

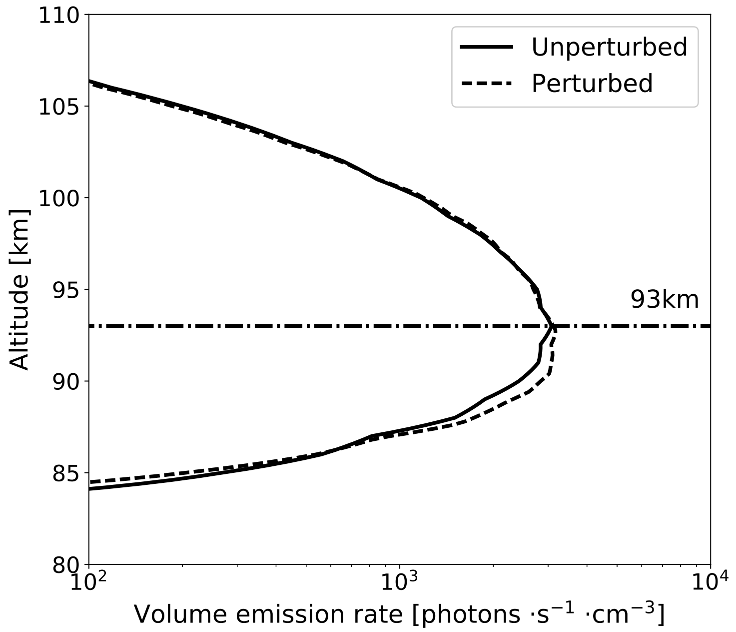


**Figure 3.** Modeled $O_2$ A-band nightglow emission profile at 30° N and 88° E for 22:00 local solar time as simulated by the HAMMONIA model. The solid curve represents an $O_2$ A-band profile for unperturbed conditions, and the dashed curve represents a profile perturbed by a GW with 15 km vertical wavelength and 5 K amplitude.

the rotational band structure of the emissions. Under thermal equilibrium conditions, the $O_2$ A-band rotational excitation follows the Boltzmann distribution at a rotational temperature $T$, which is assumed to be equal to the background temperature. The number of photons that appears in an individual rotational line is given by $\eta_{\text{rot}}$:

$$\eta_{\text{rot}} = \eta \frac{g'}{Q(T)} \exp(\frac{-hcE'}{kT}) A_1 \tag{4}$$

where $h$ is the Planck constant, $c$ is the light speed, $k$ is the Boltzmann constant. $E'$ and $g'$are the upper state energy and upper state degeneracy, respectively. $A_1$ is the Einstein coefficient of the transition. $Q(T)$ is the rotational partition function:

$$Q(T) = \sum g' \exp(\frac{-hcE'}{kT}) \tag{5}$$

A subset of six emission lines has proven to give an optimal setup for a potential satellite mission aiming to the derivation of kinetic temperature from the $O_2$ A-band. These six lines show both positive and negative temperature dependence of rotational structures, also strong, medium and weak dependence are included, as shown in Fig. 4.

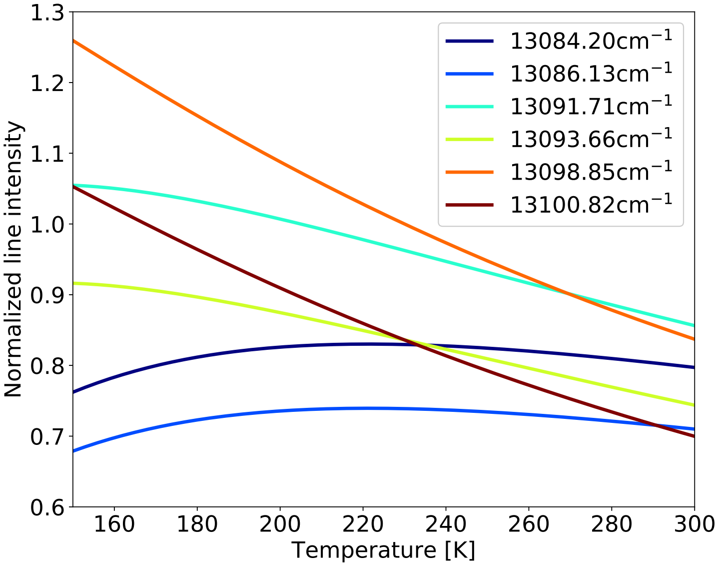


**Figure 4.** Temperature dependence of six rotational lines of the $O_2$ A-Band. The line center wavenumbers for the lines are given in the figure legend. The intensity is normalized around the maximum intensity for a temperature of 230 K.

### 3.2 Wave perturbations

$O_2$ A-band emissions are affected by gravity waves due to the vertical displacement of constituents and temperature changes associated to the waves. Following conventional assumption, we consider an adiabatic and windless atmosphere. A monochromatic wave perturbation added in background temperature $T_0$ at position $(x,z)$ can be written as:

$$T(x,z,t) = T_0(x,z,t) + A\cos\left(\frac{2\pi x}{\lambda_x} + \frac{2\pi z}{\lambda_z} - \hat{\omega}t\right) \tag{6}$$

with the wave amplitude $A$, the vertical wavelength $\lambda_z$, the horizontal wavelength $\lambda_x$ and the intrinsic frequency $\hat{\omega}$ of wave perturbation. We used the following expression (Ward, 1999) to calculate the vertical displacement $\delta z$ of an air parcel from its equilibrium height $z+\delta z$:

$$T(x,z,\delta z) \approx T(x,z) + (\Gamma_{ad} - \Gamma)\delta z \tag{7}$$

where $\Gamma$ and $\Gamma_{ad}$ are the local and adiabatic lapse rates, respectively. Then, the perturbed density (background density plus perturbation) $\rho'$ at fixed height $z$ can be calculated as density at equilibrium height $z+\delta_z$:

$$\rho'(x,z) = \rho(x,z,\delta z) \approx \rho(x,z)\exp^{-\kappa\delta z/H} \tag{8}$$

with the scale height $H$. In the quantity $\kappa = (c_p/c_v - 1)$, $c_p$ and $c_v$ represent heat capacities at constant pressure and volume, respectively. Given $\rho'$, the number densities for perturbed major gases are calculated as (Liu, 2003; Vargas et al., 2007):

$$\frac{[\mathrm{N_2}]'}{[\mathrm{N_2}]} = \frac{[\mathrm{O_2}]'}{[\mathrm{O_2}]} = \frac{\rho'}{\rho} \tag{9}$$

Because the mixing ratio of atomic oxygen is not constant with altitude, the perturbed volume mixing ratio $v'$ is calculated as follows (Ward, 1999):

$$v'_{\mathrm{O}}(x,z) = v_{\mathrm{O}}(x,z,\delta_z) \approx v_{\mathrm{O}}(x,z+\delta_z) \tag{10}$$

Figure. 3 shows a perturbed $O_2$ A-band volume emission rate profile perturbed by a 1D GW with a vertical wavelength $\lambda_z$ of 15 km and an amplitude $A$ of 5 K.

### 3.3 Ray tracing

To model the instrument's LOS in a three dimensional atmosphere we utilize a module of the Atmospheric Radiative Transfer Simulator (ARTS) (Buehler et al., 2005). ARTS is a free open-source software program that simulates atmospheric radiative transfer. It focuses on thermal radiation from the microwave to the infrared spectral range. The second version of ARTS (Eriksson et al., 2011) allows simulations for one-, two- or three-dimensional atmospheres. In this study, the relative orientations of LOS is selected to be parallel to the orbit plane. Thus, it is assumed that the LOS is in the orbit plane, and a 2D ray tracing can be applied with ARTS-2.

### 3.4 Radiative transfer

The observed spectral irradiance $I(v)$, in photons $\cdot\, \mathrm{s}^{-1} \cdot \mathrm{cm}^{-2}$, is a path integral along the line-of-sight:

$$I(v) = \int_{-\infty}^{\infty} \eta(s)_{\mathrm{rot}}\, D(v,s)\, \exp[-\int_{-s}^{\infty} n(s')\, \sigma(s')\, ds']\, ds \tag{11}$$

where $s$ is the distance along the line-of-sight, $n$ is the $O_2$ number density, $\sigma$ is the absorption cross section, and $D(v)$ is the Doppler line shape for the spectral line centered at wavenumber $v$. In the infrared the lower atmosphere is optically thick, whereas the upper atmosphere can be considered as optically thin. Since the $O_2$ A-Band is a transition to the $O_2$ ground state, the atmosphere becomes optically thick at stratopause altitudes. Therefore, any emission from the Earth's surface or tropospheric altitudes cannot reach the upper mesosphere at these wavelengths. At nightglow layer altitudes (upper mesosphere / lower thermosphere) the atmosphere is optically thin for the wavelengths considered. In our case, for altitudes above 85 km, the atmosphere is assumed to be optically thin and the self-absorption term can be omitted (Sheese, 2011).

The spectral range considered in this work is 13082-13103 $\mathrm{cm}^{-1}$ and contains six emission lines. The central wavenumbers of these lines are given in Fig. 4. In Fig. 5, limb radiance spectra are simulated at different altitudes (86-115.5 km with 1.5 km interval). To make a trade-off between bandwidth and instrument size, a spectral resolution of 0.8 $\mathrm{cm}^{-1}$ is chosen. The temperature dependence of the lines in this spectral interval is illustrated in Fig. 4.

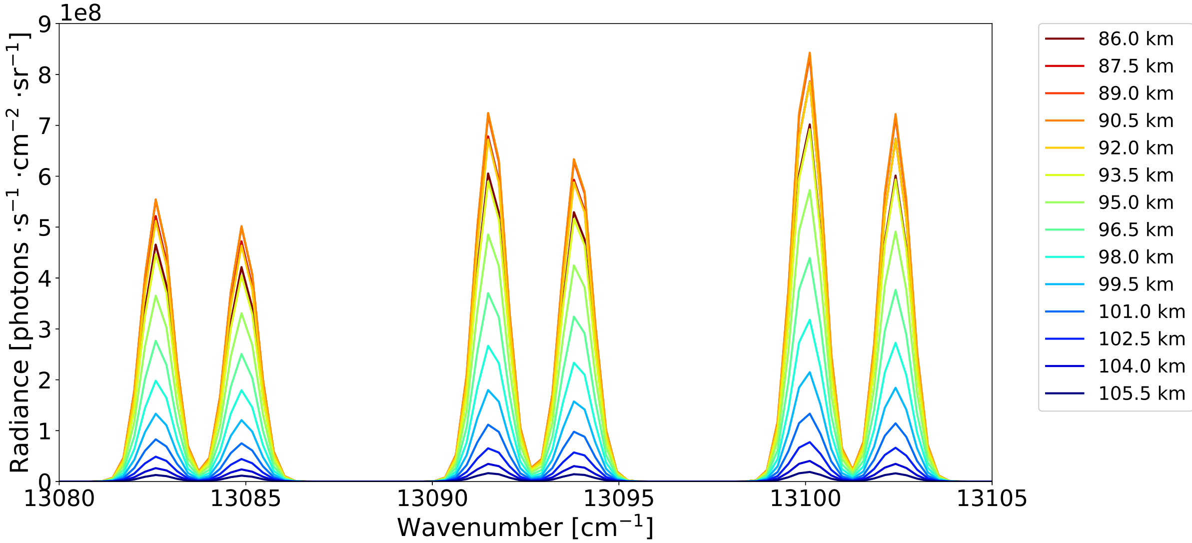


**Figure 5.** Modeled limb spectra for different tangent altitudes. The background atmosphere is taken from the HAMMONIA model, around 30° N and 88° E for 22:00 local solar time.

## 4 Retrieval model

The tomographic retrieval presented here is similar to the widely used optimal estimation approach (Rodgers, 2004). The measurement space is represented by vector $\boldsymbol{y}$ and the unknown atmospheric state is represented by vector $\boldsymbol{x}$. The forward model $\boldsymbol{f}(\boldsymbol{x})$ provides the simulated spectrum based on a given atmospheric state $\boldsymbol{x}$:

$$\boldsymbol{y} = \boldsymbol{f}(\boldsymbol{x}) + \boldsymbol{\epsilon} \tag{12}$$

where $\boldsymbol{\epsilon}$ is the measurement error. The inversion problem of Eq. (12) is generally ill-posed, and the solution is not unique. Following Tikhonov and Arsenin (1977) and Rodgers (2004), the cost function $\boldsymbol{J}$ is complemented by a regularization term:

$$\boldsymbol{J}(\boldsymbol{x}) = (\boldsymbol{f}(\boldsymbol{x}) - \boldsymbol{y})^T \mathbf{S}_\epsilon^{-1} (\boldsymbol{f}(\boldsymbol{x}) - \boldsymbol{y}) + (\boldsymbol{x} - \boldsymbol{x_a})^T \mathbf{S}_a^{-1} \mathbf{R} (\boldsymbol{x} - \boldsymbol{x_a}) \tag{13}$$

where matrix ~~$\mathbf{S}_a^{-1}$~~ $\mathbf{R}$ is the inverse covariance or regularization matrix, $\mathbf{S}_\epsilon$ is the covariance matrix of the measurement error, and $\boldsymbol{x_a}$ represents the a priori data. The a priori data is usually taken as the climatological mean of the retrieved quantities. ~~It~~ The second term in the cost function (Eq. (13)) ensures that a unique and physically meaningful solution can be obtained. The inversion of the forward model (Eq. (12)) can be formulated as a minimization of the cost function $\boldsymbol{J}(\boldsymbol{x})$ given in Eq. (13). To solve the non-linear minimization, we adopt a Levenberg-Marquardt iteration scheme (Levenberg, 1944; Marquardt, 1963; Ceccherini and Ridolf

### 4.1 2-dimensional regularization matrix

The design of the 2-dimensional regularization matrix $\cancel{\mathbf{S}_a^{-1}}$ $\mathbf{R}$ in Eq. (13) is of considerable importance to the retrieval results. Here, we used a combination of zeroth and first order Tikhonov regularization (Tikhonov and Arsenin, 1977):

$$\mathbf{S}_a^{-1}\mathbf{R} = (\alpha_0 \mathbf{L}_0^T \mathbf{L}_0 + \alpha_1^x \mathbf{L}_1^{x\,T} \mathbf{L}_1^x + \alpha_1^y \mathbf{L}_1^{y\,T} \mathbf{L}_1^y) \tag{14}$$

where the weighting parameters $\alpha_0$, $\alpha_1^x$ and $\alpha_1^y$ control the overall strength of the regularization term added in Eq. (13). Large values of weighting parameters will result in an over-regularized result, while a small value will give ~~a noisy or no~~ an unstable solution. The parameter $\alpha_0$, $\alpha_1^x$ and $\alpha_1^y$ also balance the contribution of the zeroth and the two directional first order regularization terms. $\mathbf{L}_0$ is an identity matrix that constrains the result to the absolute value of $\boldsymbol{x}_a$. Matrix $\mathbf{L}_1$ maps $\boldsymbol{x}$ onto its first order derivative in the vertical and horizontal directions:

$$\mathbf{L}_1^x(i,j) = \begin{cases} 1 & \text{if } j = i+1 \\ -1 & \text{if } j = i \\ 0 & \text{otherwise} \end{cases}, \quad \mathbf{L}_1^y(i,j) = \begin{cases} 1 & \text{if } j = i+m \\ -1 & \text{if } j = i \\ 0 & \text{otherwise} \end{cases} \tag{15}$$

As we convert the 2D atmospheric temperature to a vector $\boldsymbol{x}$ row by row, $\mathbf{L}_1^x$ is thus a $(l-1)\times l$ matrix with $l$ to be the number of elements in $\boldsymbol{x}$. $\mathbf{L}_1^y$ is a $(l-m)\times l$ matrix with $m$ to be the number of elements contained in each row of the 2D atmospheric volume.

### 4.2 Averaging kernel matrix.

Following the concept of Rodgers (2004), the effect of the regularization onto the retrieval result can be quantified by the averaging kernel (AVK) matrix:

$$\mathbf{A} = (\mathbf{S}_a^{-1}\mathbf{R} + {}'()\mathbf{K}^T \mathbf{S}_\epsilon^{-1}{}'()\mathbf{K})^{-1}{}'()\mathbf{K}^T \mathbf{S}_\epsilon^{-1}{}'()\mathbf{K} \tag{16}$$

where $\cancel{\boldsymbol{f}'}$ $\mathbf{K}$ is the Jacobian ~~matrix~~ of the forward model $\boldsymbol{f}$ at atmospheric state $\boldsymbol{x}$. The measurement contribution vector can be obtained from the AVK by the sum over each row of $\mathbf{A}$. If the measurement contribution value is close to 1, most information of the retrieval result is determined by the measurements and not by the absolute value of the a priori data. The averaging kernel matrix can also be used to deduce the spatial resolution of retrieval result. For 1D retrievals, the vertical resolution is described by calculating the full width at half maximum (FWHM) of the corresponding row of the AVK matrix. For 2D retrievals, the row needs first to be reshaped into two dimensions, and then the FWHM method is used to calculate the resolution along each axis (Steck et al., 2005).

## 5 Numerical experiments

### 5.1 Simulation setup

In this section, we present the experimental results of tomographic temperature retrievals using simulated 'target mode' measurements with $1\%$ noise added. Synthetic measurements are generated by imprinting a gravity wave structure onto a smooth model atmosphere, as described in Sect. 3.2. The temperature, atmospheric density and concentrations of various constituents are perturbed by this simulated wave. As the amplitude is the most important feature of a GW with respect to energy, the assessment in the next step focuses on how well the wave amplitude can be reproduced from the retrieval results. The wave vector investigated in this case is assumed along the direction of line-of-sight, where the largest amplitude suppression is provided (Preusse et al., 2009b).

In our study, the spacing of the atmospheric grids is very important for both the forward and the retrieval model. To reduce the impact of the discretization on the synthetic measurements, the atmospheric grid in the forward model should be finely sampled. The atmospheric grid used in the forward model has a vertical spacing of 250 m and horizontal spacing of 5 km. In the inverse procedure, the sampling can be coarser: 500 m vertical spacing and 12.5 km horizontal spacing in our case.

### 5.2 Example of a gravity wave parameter retrieval

Figure. 6 illustrates the performance of the tomographic retrieval approach for an atmosphere disturbed by a gravity wave with a horizontal and vertical wavelength of 300 km and 15 km, respectively. The satellite platform is simulated in an approximately 600 km sun-synchronous orbit with an inclination angle of 98°. The instrument will employ a 2D detector array consisting of about 40 × 400 super pixels. It measures in the spectral regions from 13082 to 13103 $\mathrm{cm}^{1}$ within the altitude range from ≈60 to 120 km in limb imaging measurements. The atmospheric condition as well as the sampling patterns are the same as in the previous sections. The integration time is assumed to be 10 seconds for limb measurements and 15 seconds for sub-limb measurements. The a-priori data used in this case study is depicted in Fig. 6 (a). The simulated gravity wave has an amplitude of 5 K (Fig. 6 (b)). The retrieved temperature perturbation is shown in Fig. 6 (c). We can clearly see that the wave structure is well reproduced between 87 and 104 km height. The horizontal coverage of such a group of 'target mode' measurements is around 800 km. Fig. 6 (d) depicts the difference between simulated wave and retrieved wave, with an average error of about 0.5 K.

The spatial resolution of the retrieved data is usually described by the rows of the averaging kernel matrix, $\mathbf{A}$. The deviation of $\mathbf{A}$ from the identity matrix gives insight into the smoothing introduced by the regularization. For example, if two adjacent grid points share one piece of information, the corresponding information content would be 0.5. By reordering a single row of $\mathbf{A}$ according to their vertical and horizontal coordinates, the influence of each point on the retrieval result can be revealed. Fig. 7 shows the 2-D averaging kernel matrix of two selected data points, which are marked as black dots in Fig. 6 (c).

Figure. 7 (a) shows the averaging kernel matrix for a point positioned at 2100 km along track and 95 km altitude. It indicates that the measurement contribution is sharply centered around this point. A minor part of the information comes from other altitudes on parabola shaped tracks, which corresponds to the line-of-sights of observations, whose tangent altitude is below

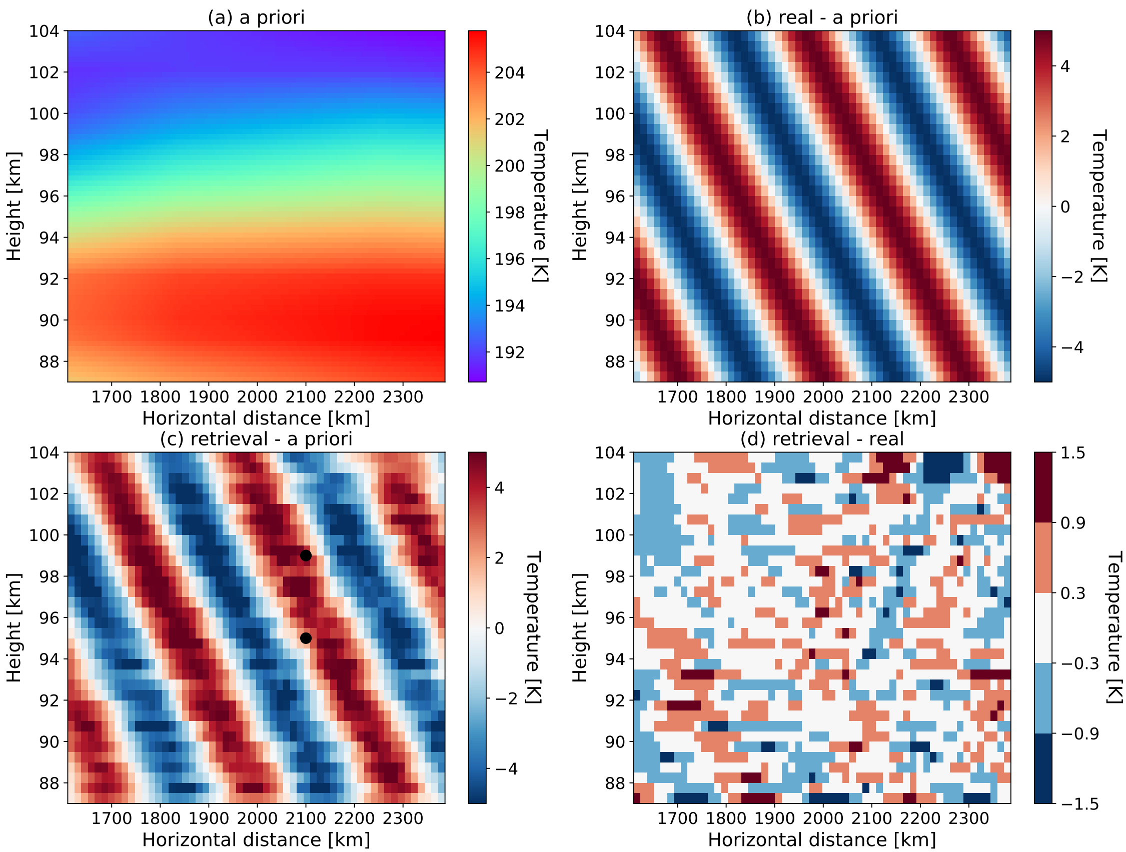


**Figure 6.** Retrieval result using simulated data. The background atmosphere is taken from the HAMMONIA run between 30° N and 36° N, 90° E, around 22:00 local solar time. The a priori atmosphere is depicted in panel (a). The difference between the perturbed atmosphere and the a priori is shown in panel (b). The retrieved wave perturbation, which is obtained by subtracting the a priori from the retrieval result, is given in panel (c). The two black dots correspond to the retrieval points selected for Fig. 7. The difference between the retrieval result and the true state of atmosphere is shown in panel (d).

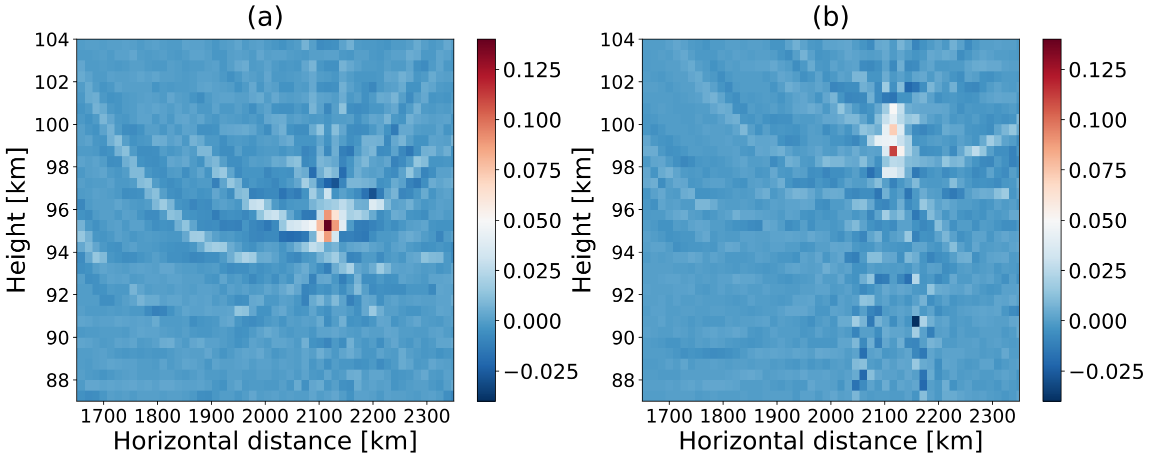


**Figure 7.** Averaging kernel matrix for two different retrieval points, allocated at the geographical position of highest values (red color). Figure (a) is for a point coinciding with the observational grid, whereas Figure (b) shows a point, whose vertical position is in between two tangent altitudes of the limb observations; for details see text.

95 km or which are sub-limb observations. For Fig. 7 (b), the data point is placed at 2100 km along track and 99 km altitude. In contrast to Figure (a), this data point is not right on the tangent altitude of an observation, but in-between two observations. Because this point is not placed exactly at one of the tangent altitudes, main contributions to the retrieved value come from measurements of adjacent grid points. According to Fig. 7 (a), a vertical resolution of 1.3 km and horizontal resolution of 35 km can be achieved.

### 5.3 Sensitivity study

The quality of a gravity wave amplitude-, wavelength- and phase- retrieval depends on the wavelength of the wave. The long LOS of limb observations is ideal for the reconstruction of long horizontal wavelengths, whereas gravity waves with short horizontal wavelengths are likely underestimated or cannot be measured at all. A measure to assess the sensitivity of an observation system to retrieve gravity wave parameters is the so called gravity wave sensitivity function (Preusse et al., 2002). It defines how a wave perturbation of a given horizontal and vertical wavelength is reproduced by a retrieval. One option to determine this gravity wave sensitivity function is to perform the retrieval for the wavelength of interest. However, for a tomographic retrieval this is computationally very expensive. Alternatively, we can derive the gravity wave sensitivity function more efficiently by using the averaging kernel matrix method (Ungermann et al., 2010a). The basic idea of this method is to assume that the forward model can be approximated linearly for a small perturbation as induced by a gravity wave. In this case, the averaging kernel matrix $\mathbf{A}$ would be identical for the unperturbed atmosphere and the perturbed atmosphere. If the unperturbed atmosphere $\boldsymbol{x}_b$ is assumed to be the same as the a priori data $\boldsymbol{x}_a$, the retrieval result $\boldsymbol{x}_f$ and the a priori vector $\boldsymbol{x}_a$

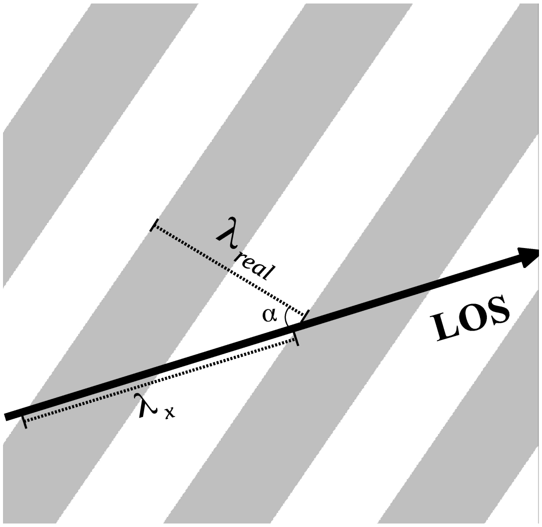


**Figure 8.** Viewing geometry between the satellite line-of-sight (LOS) and the horizontal wave vector. The wave fronts are represented by the gray shading. The observed horizontal wavelength $\lambda_x$ and the real horizontal wavelength $\lambda_{\mathrm{real}}$ are related by an angle $\alpha$: $\lambda_{\mathrm{real}} = \lambda_x \cos\alpha$.

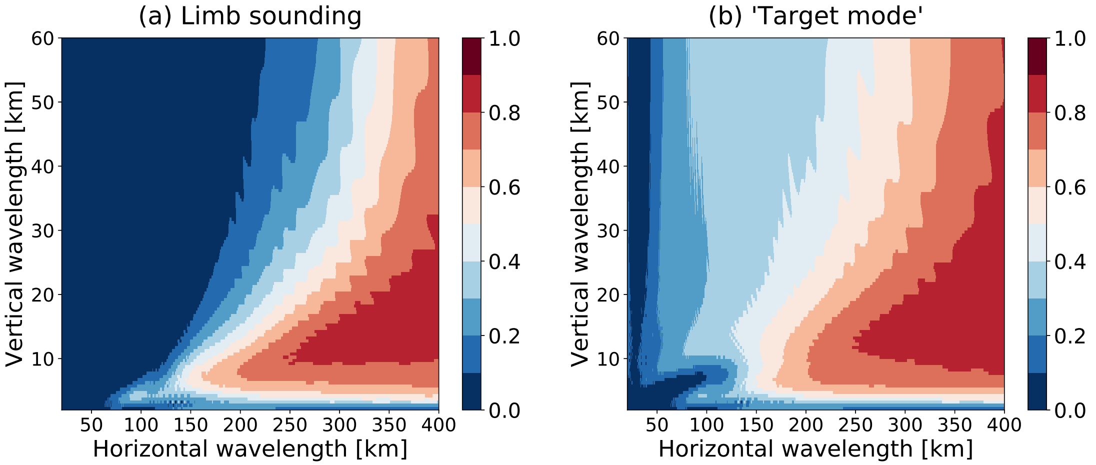


**Figure 9.** Gravity wave sensitivity function. The ratio of retrieved wave amplitude to true wave amplitude as function of horizontal and vertical wavelength is shown. Figure (a) is the sensitivity function for pure limb measurements, whereas Figure (b) is for 'target mode' measurements as specified in Sect. 5.

are related as follows:

$$\boldsymbol{x}_f - \boldsymbol{x}_a = (\mathbf{A}(\boldsymbol{x}_a + \boldsymbol{x}_\delta) + (\mathbf{I} - \mathbf{A})\boldsymbol{x}_a) - \boldsymbol{x}_a = \mathbf{A}\boldsymbol{x}_\delta \quad (17)$$

with $\mathbf{I}$ being the identity matrix and $\boldsymbol{x}_\delta$ being the modulated wave structure. Following this equation, the averaging kernel matrix $\mathbf{A}$ maps the true wave perturbations $\boldsymbol{x}_\delta$ onto the retrieved wave structure $\boldsymbol{x}_f - \boldsymbol{x}_a$. The ratio between $\boldsymbol{x}_f - \boldsymbol{x}_a$ and $\boldsymbol{x}_\delta$ quantifies the sensitivity to reconstruct the gravity wave.

For this 'target mode', the observed horizontal wavelength is the wavelength projected along the LOS. In general, there is an angle $\alpha$ between the LOS and the horizontal wave vector. Therefore, the observed horizontal wavelength $\lambda_x$ is a factor of $1/(\cos\alpha)$ larger than the real horizontal wavelength $\lambda_{\text{real}}$, as illustrated in Fig. 8. In this sensitivity study, the horizontal wavelength discussed is the observed horizontal wavelength $\lambda_x$.

Fig. 9 shows the results of sensitivity study adopting this approach for horizontal and vertical wavelengths of 0-400 and 0-60 km, respectively. To illustrate the advancement of the combination of limb and sub-limb observations for the reconstruction of gravity wave amplitudes, the sensitivity function for a pure limb measurement was also calculated, as shown in Fig. 9 (a). The retrieval setup is the same for both cases, but the additional sub-limb measurements were removed from Fig. 9 (b) to get pure limb simulation in Fig. 9 (a).

For pure limb sounding, GWs with vertical and horizontal wavelengths down to 7 km and 150 km, respectively, can be observed. The sensitivity to detect short horizontal wavelengths decreases for larger vertical wavelengths, e.g. 250 km at 20 km vertical wavelength, or 325 km at 60 km vertical wavelength, respectively. In Fig. 9 (b), 'target mode' tomography has been performed which considers sub-limb measurements with 15 seconds integration time as well. The GW sensitivity function does not change much for short vertical wavelength compared to pure limb measurements, but gravity waves with large vertical wavelength and short horizontal wavelength become much more visible. For GWs with vertical wavelengths above 15 km, the increase in horizontal wavelength sensitivity is typically 50-100 km. Another advancement of the 'target mode' is the reduced altitude dependence of the observational filter, as it is also illustrated in Fig. 10 for a GW with 250 km horizontal wavelength and 40 km vertical wavelength. Comparing the retrieved wave structure with the true structure (depicted as the black contour plot), the 'target mode' tomography can reconstruct the wave structure more clearly than the limb mode tomography.

## 6 Conclusion

In recent years, tomographic retrieval approaches have been proposed to reconstruct 2D gravity wave structures. However, the spatial resolution of gravity waves retrieved from this observation mode is limited by the poor horizontal resolution along the instrument's LOS of these instruments.

In this paper, a novel 'target mode' observation combining limb and sub-limb measurements for retrieval of GW parameters in the mesopause region is presented. A tailored retrieval scheme for this observational mode has been presented and its performance has been assessed.

We employed this new approach to simulated measurements of an instrument measuring the $O_2$ A-band nightglow emissions to demonstrate its advantages in resolving 2D atmospheric structures. The retrieval results show that a combination of limb

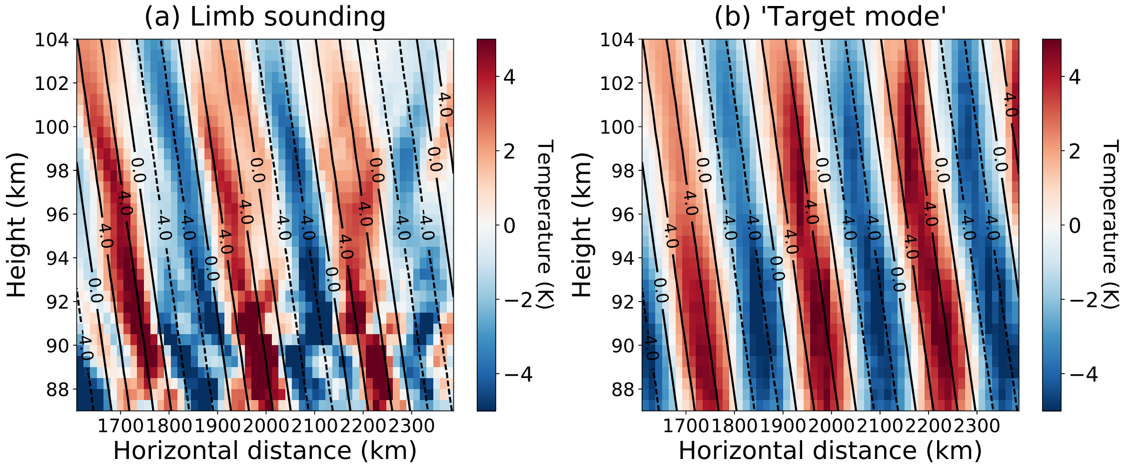


**Figure 10.** Pure limb sounding (a) and 'target mode' (b) retrieval results comparison. The gravity wave has a wavelength of 250 km in horizontal and 40 km in vertical. The climatological background profile was subtracted from the retrieval result. The black lines indicate the true modulated wave structure.

and sub-limb measurements increases the sensitivity to detect short horizontal wavelengths by 50-100 km compared to pure limb sounding. GWs with vertical and horizontal wavelength down to 7 km and 150 km can be resolved. It is shown that its capability of detecting short horizontal wavelength is depending on the vertical wavelength of GWs, e.g. 200 km at 20 km vertical wavelength, and 260 km at 60 km vertical wavelength, respectively.


## 5 Acknowledgements

This work was supported in part by the National Natural Science Foundation of China under Grants 41590852, and the China scholarship council (201404910513).

## References


Alexander, M. J. and Barnet, C.: Using Satellite Observations to Constrain Parameterizations of Gravity Wave Effects for Global Models, Journal of the Atmospheric Sciences, 64, 1652–1665, doi:10.1175/JAS3897.1, 2007.

Alexander, M. J., Gille, J., Cavanaugh, C., Coffey, M., Craig, C., Eden, T., Francis, G., Halvorson, C., Hannigan, J., Khosravi, R., Kinnison, D., Lee, H., Massie, S., Nardi, B., Barnett, J., Hepplewhite, C., Lambert, A., and Dean, V.: Global estimates of gravity wave momentum flux from High Resolution Dynamics Limb Sounder observations, Journal of Geophysical Research: Atmospheres, 113, doi:10.1029/2007JD008807, d15S18, 2008.

Buehler, S., Eriksson, P., Kuhn, T., von Engeln, A., and Verdes, C.: ARTS, the atmospheric radiative transfer simulator, Journal of Quantitative Spectroscopy and Radiative Transfer, 91, 65–93, doi:10.1016/j.jqsrt.2004.05.051, 2005.

Burrage, M. D., Arvin, N., Skinner, W. R., and Hays, P. B.: Observations of the $O_2$ atmospheric band nightglow by the high resolution Doppler imager, Journal of Geophysical Research, 99, 15 017, doi:10.1029/94JA00791, 1994.

Campbell, I. and Gray, C.: Rate constants for O($^3P$) recombination and association with N($^4S$), Chemical Physics Letters, 18, 607–609, doi:10.1016/0009-2614(73)80479-8, 1973.

Carlotti, M., Dinelli, B. M., Raspollini, P., and Ridolfi, M.: Geo-fit approach to the analysis of limb-scanning satellite measurements, Applied optics, 40, 1872–1885, doi:10.1364/ORS.2001.OWC5, 2001.

Ceccherini, S. and Ridolfi, M.: Technical Note: Variance-covariance matrix and averaging kernels for the Levenberg-Marquardt solution of the retrieval of atmospheric vertical profiles, Atmospheric Chemistry and Physics, 10, 3131–3139, doi:10.5194/acp-10-3131-2010, 2010.

Eckermann, S. D. and Preusse, P.: Global Measurements of Stratospheric Mountain Waves from Space, Science, 286, 1534–1537, doi:10.1126/science.286.5444.1534, 1999.

Eriksson, P., Buehler, S., Davis, C., Emde, C., and Lemke, O.: ARTS, the atmospheric radiative transfer simulator, version 2, Journal of Quantitative Spectroscopy and Radiative Transfer, 112, 1551–1558, doi:10.1016/j.jqsrt.2011.03.001, 2011.

Ern, M., Preusse, P., Alexander, M. J., and Warner, C. D.: Absolute values of gravity wave momentum flux derived from satellite data, Journal of Geophysical Research: Atmospheres, 109, doi:10.1029/2004JD004752, d20103, 2004.

Ern, M., Lehmann, C., Kaufmann, M., and Riese, M.: Spectral wave analysis at the mesopause from SCIAMACHY airglow data compared to SABER temperature spectra, Annales Geophysicae, 27, 407–416, doi:10.5194/angeo-27-407-2009, 2009.

Ern, M., Preusse, P., Gille, J. C., Hepplewhite, C. L., Mlynczak, M. G., Russell, J. M., and Riese, M.: Implications for atmospheric dynamics derived from global observations of gravity wave momentum flux in stratosphere and mesosphere, Journal of Geophysical Research: Atmospheres, 116, doi:10.1029/2011JD015821, d19107, 2011.

Ern, M., Hoffmann, L., and Preusse, P.: Directional gravity wave momentum fluxes in the stratosphere derived from high-resolution AIRS temperature data, Geophysical Research Letters, 44, 475–485, doi:10.1002/2016GL072007, 2016GL072007, 2017.

Fetzer, E. J. and Gille, J. C.: Gravity Wave Variance in LIMS Temperatures. Part I: Variability and Comparison with Background Winds, Journal of the Atmospheric Sciences, 51, 2461–2483, doi:10.1175/1520-0469(1994)051<2461:GWVILT>2.0.CO;2, 1994.

Fetzer, E. J. and Gille, J. C.: Gravity Wave Variance in LIMS Temperatures. Part II: Comparison with the Zonal-Mean Momentum Balance, Journal of the Atmospheric Sciences, 53, 398–410, doi:10.1175/1520-0469(1996)053<0398:GWVILT>2.0.CO;2, 1996.

Forbes, J. M., Russell, J., Miyahara, S., Zhang, X., Palo, S., Mlynczak, M., Mertens, C. J., and Hagan, M. E.: Troposphere-thermosphere tidal coupling as measured by the SABER instrument on TIMED during July–September 2002, Journal of Geophysical Research: Space Physics, 111, doi:10.1029/2005JA011492, a10S06, 2006.

Fritts, D. C. and Alexander, M. J.: Gravity wave dynamics and effects in the middle atmosphere, Reviews of Geophysics, 41, doi:10.1029/2001RG000106, 1003, 2003.

Fritts, D. C., Pautet, P.-D., Bossert, K., Taylor, M. J., Williams, B. P., Iimura, H., Yuan, T., Mitchell, N. J., and Stober, G.: Quantifying gravity wave momentum fluxes with Mesosphere Temperature Mappers and correlative instrumentation, Journal of Geophysical Research: Atmospheres, 119, 13,583–13,603, doi:10.1002/2014JD022150, 2014JD022150, 2014.

Garcia, R. R. and Solomon, S.: The effect of breaking gravity waves on the dynamics and chemical composition of the mesosphere and lower thermosphere, Journal of Geophysical Research, 90, 3850, doi:10.1029/JD090iD02p03850, 1985.

Gong, J., Wu, D. L., and Eckermann, S. D.: Gravity wave variances and propagation derived from AIRS radiances, Atmospheric Chemistry and Physics, 12, 1701–1720, doi:10.5194/acp-12-1701-2012, 2012.

Greer, R., Llewellyn, E., Solheim, B., and Witt, G.: The excitation of $O_2(b_1\Sigma_g^+)$ in the nightglow, Planetary and Space Science, 29, 383–389, doi:10.1016/0032-0633(81)90081-7, 1981.

Hoffmann, L. and Alexander, M. J.: Retrieval of stratospheric temperatures from Atmospheric Infrared Sounder radiance measurements for gravity wave studies, Journal of Geophysical Research: Atmospheres, 114, doi:10.1029/2008JD011241, d07105, 2009.

Hoffmann, L., Grimsdell, A. W., and Alexander, M. J.: Stratospheric gravity waves at Southern Hemisphere orographic hotspots: 2003–2014 AIRS/Aqua observations, Atmospheric Chemistry and Physics, 16, 9381–9397, doi:10.5194/acp-16-9381-2016, 2016.

Holton, J. R.: The Role of Gravity Wave Induced Drag and Diffusion in the Momentum Budget of the Mesosphere, Journal of the Atmospheric Sciences, 39, 791–799, doi:10.1175/1520-0469(1982)039<0791:TROGWI>2.0.CO;2, 1982.

Kaufmann, M., Blank, J., Guggenmoser, T., Ungermann, J., Engel, A., Ern, M., Friedl-Vallon, F., Gerber, D., Grooß, J. U., Guenther, G., Höpfner, M., Kleinert, A., Kretschmer, E., Latzko, T., Maucher, G., Neubert, T., Nordmeyer, H., Oelhaf, H., Olschewski, F., Orphal, J., Preusse, P., Schlager, H., Schneider, H., Schuettemeyer, D., Stroh, F., Suminska-Ebersoldt, O., Vogel, B., M. Volk, C., Woiwode, W., and Riese, M.: Retrieval of three-dimensional small-scale structures in upper-tropospheric/lower-stratospheric composition as measured by GLORIA, Atmospheric Measurement Techniques, 8, 81–95, doi:10.5194/amt-8-81-2015, 2015.

Levenberg, K.: A method for the solution of certain non-linear problems in least squares, Quarterly of Applied Mathematics, 2, 164–168, 1944.

Lindzen, R. S.: Turbulence and stress owing to gravity wave and tidal breakdown, Journal of Geophysical Research, 86, 9707, doi:10.1029/JC086iC10p09707, 1981.

Liu, A. Z.: A modeling study of $O_2$ and OH airglow perturbations induced by atmospheric gravity waves, Journal of Geophysical Research, 108, doi:10.1029/2002JD002474, 2003.

Livesey, N. J. and Read, W. G.: Direct retrieval of line-of-sight atmospheric structure from limb sounding observations, Geophysical Research Letters, 27, 891–894, doi:10.1029/1999GL010964, 2000.

Marquardt, D. W.: An Algorithm for Least-Squares Estimation of Nonlinear Parameters, Journal of the Society for Industrial and Applied Mathematics, 11, 431–441, doi:10.1137/0111030, 1963.

McDade, I., Murtagh, D., Greer, R., Dickinson, P., Witt, G., Stegman, J., Llewellyn, E., Thomas, L., and Jenkins, D.: ETON 2: Quenching parameters for the proposed precursors of $O_2(b_1\Sigma_g^+)$ and O($^1$S) in the terrestrial nightglow, Planetary and Space Science, 34, 789–800, doi:10.1016/0032-0633(86)90075-9, 1986.

Preusse, P., Dörnbrack, A., Eckermann, S. D., Riese, M., Schaeler, B., Bacmeister, J. T., Broutman, D., and Grossmann, K. U.: Space-based measurements of stratospheric mountain waves by CRISTA 1. Sensitivity, analysis method, and a case study, Journal of Geophysical Research: Atmospheres, 107, doi:10.1029/2001JD000699, 8178, 2002.

Preusse, P., Eckermann, S. D., Ern, M., Oberheide, J., Picard, R. H., Roble, R. G., Riese, M., Russell, J. M., and Mlynczak, M. G.: Global ray tracing simulations of the SABER gravity wave climatology, Journal of Geophysical Research: Atmospheres, 114, doi:10.1029/2008JD011214, d08126, 2009a.

Preusse, P., Schroeder, S., Hoffmann, L., Ern, M., Friedl-Vallon, F., Ungermann, J., Oelhaf, H., Fischer, H., and Riese, M.: New perspectives on gravity wave remote sensing by spaceborne infrared limb imaging, Atmospheric Measurement Techniques, 2, 299–311, doi:10.5194/amt-2-299-2009, 2009b.

Riese, M., Oelhaf, H., Preusse, P., Blank, J., Ern, M., Friedl-Vallon, F., Fischer, H., Guggenmoser, T., Höpfner, M., Hoor, P., Kaufmann, M., Orphal, J., Plöger, F., Spang, R., Suminska-Ebersoldt, O., Ungermann, J., Vogel, B., and Woiwode, W.: Gimballed Limb Observer for Radiance Imaging of the Atmosphere (GLORIA) scientific objectives, Atmospheric Measurement Techniques, 7, 1915–1928, doi:10.5194/amt-7-1915-2014, 2014.

Rodgers, C. D.: Inverse methods for atmospheric sounding: theory and practice, no. 2 in Series on atmospheric oceanic and planetary physics, World Scientific, Singapore, reprinted edn., 2004.

Schmidt, H., Brasseur, G. P., Charron, M., Manzini, E., Giorgetta, M. A., Diehl, T., Fomichev, V. I., Kinnison, D., Marsh, D., and Walters, S.: The HAMMONIA Chemistry Climate Model: Sensitivity of the Mesopause Region to the 11-Year Solar Cycle and $CO_2$ Doubling, Journal of Climate, 19, 3903–3931, doi:10.1175/JCLI3829.1, 2006.

Sheese, P.: Mesospheric ozone densities retrieved from OSIRIS observations of the $O_2$ A-band dayglow, Ph.D. thesis, Library and Archives Canada = Bibliothèque et Archives Canada, Ottawa, 2011.

Steck, T., Höpfner, M., von Clarmann, T., and Grabowski, U.: Tomographic retrieval of atmospheric parameters from infrared limb emission observations, Applied Optics, 44, 3291, doi:10.1364/AO.44.003291, 2005.

Tikhonov, A. N. and Arsenin, V. I.: Solutions of ill-posed problems, Scripta series in mathematics, Winston ; distributed solely by Halsted Press, Washington : New York, 1977.

Tsuda, T., Nishida, M., Rocken, C., and Ware, R. H.: A Global Morphology of Gravity Wave Activity in the Stratosphere Revealed by the GPS Occultation Data (GPS/MET), Journal of Geophysical Research: Atmospheres, 105, 7257–7273, doi:10.1029/1999JD901005, 2000.

Ungermann, J., Hoffmann, L., Preusse, P., Kaufmann, M., and Riese, M.: Tomographic retrieval approach for mesoscale gravity wave observations by the PREMIER Infrared Limb-Sounder, Atmospheric Measurement Techniques, 3, 339–354, doi:10.5194/amt-3-339-2010, 2010a.

Ungermann, J., Kaufmann, M., Hoffmann, L., Preusse, P., Oelhaf, H., Friedl-Vallon, F., and Riese, M.: Towards a 3-D tomographic retrieval for the air-borne limb-imager GLORIA, Atmospheric Measurement Techniques, 3, 1647–1665, doi:10.5194/amt-3-1647-2010, 2010b.

Ungermann, J., Blank, J., Lotz, J., Leppkes, K., Hoffmann, L., Guggenmoser, T., Kaufmann, M., Preusse, P., Naumann, U., and Riese, M.: A 3-D tomographic retrieval approach with advection compensation for the air-borne limb-imager GLORIA, Atmospheric Measurement Techniques, 4, 2509–2529, doi:10.5194/amt-4-2509-2011, 2011.

Vallance Jones, A.: Aurora Geophysics and Astrophysics Monographs, D. Reidel, Hingham, Mass, 1974.

Vargas, F., Swenson, G., Liu, A., and Gobbi, D.: $O(^1S)$, OH, and $O_2(b)$ airglow layer perturbations due to AGWs and their implied effects on the atmosphere, Journal of Geophysical Research, 112, doi:10.1029/2006JD007642, 2007.

Vincent, R. A.: The dynamics of the mesosphere and lower thermosphere: a brief review, Progress in Earth and Planetary Science, 2, doi:10.1186/s40645-015-0035-8, 2015.

von Clarmann, T., De Clercq, C., Ridolfi, M., Höpfner, M., and Lambert, J.-C.: The horizontal resolution of MIPAS, Atmospheric Measurement Techniques, 2, 47–54, doi:10.5194/amt-2-47-2009, 2009.

Ward, W. E.: A simple model of diurnal variations in the mesospheric oxygen nightglow, Geophysical Research Letters, 26, 3565–3568, doi:10.1029/1999GL003661, 1999.

Wright, C. J., Osprey, S. M., Barnett, J. J., Gray, L. J., and Gille, J. C.: High Resolution Dynamics Limb Sounder measurements of gravity wave activity in the 2006 Arctic stratosphere, Journal of Geophysical Research: Atmospheres, 115, doi:10.1029/2009JD011858, d02105, 2010.

Wu, D. L.: Mesoscale gravity wave variances from AMSU-A radiances, Geophysical Research Letters, 31, doi:10.1029/2004GL019562, l12114, 2004.

Wu, D. L. and Waters, J. W.: Gravity-wave-scale temperature fluctuations seen by the UARS MLS, Geophysical Research Letters, 23, 3289–3292, doi:10.1029/96GL02924, 1996.